UNDRAINED CYCLIC TORSIONAL SHEAR BEHAVIOR OF SATURATED SAND WITH INITIAL STATIC SHEAR

Gabriele CHIARO[1], Takashi KIYOTA[2], L.I.N. DE SILVA[3],
Takeshi SATO[4] and Junichi KOSEKI[5]

ABSTRACT: This paper summarizes the experimental results of a study conducted in order to investigate the effect of initial static shear on the undrained cyclic behavior of saturated sand under cyclic torsional shear loading up to single amplitude shear strain of about 50 %. Several hollow cylinder specimens at relative density of about 45 % were performed with varying the initial static shear and the subsequent cyclic shear stress levels. The observed failure behavior of specimens could be distinguished into liquefaction and residual deformation failures depending on the magnitude of combined static and cyclic shear stress. In addition, it was found that the presence of static shear does not always lead to an increase in the resistances to liquefaction and strain accumulation. They could either increase or decrease with increasing the static shear depending on the magnitude of combined shear stress, the type of loading and the failure behavior.

Key Words: large strain, liquefaction, residual deformation, sand, static shear stress, torsional shear loading, undrained cyclic behavior

INTRODUCTION

Experience from past large-magnitude earthquake events (e.g., 1964 Niigata Earthquake and 1983 Nihonkai-Chubu Earthquake) indicated that extremely large horizontal ground deformation can occur in liquefied sandy deposits in coastal or river areas. When lateral spreading and flow slide take place, ground movement may exceed several meters, even in gentle slopes with an inclination of less than a few percent, resulting in severe damage to buildings, infrastructures and lifeline facilities (Hamada et al., 1994).

   In sloped ground or level ground underneath structures, soil elements are subjected to an initial static shear stress on horizontal plane. During earthquake shaking, these elements are subjected to additional cyclic shear stress due to shear waves propagating vertically upward from bedrock. The superimposition of static and cyclic shear stresses can have major effect on the response of soil, leading to liquefaction and development of extremely large ground deformation.

   As far as the authors have investigated in the literature, there exists no previous study on the role of initial static shear stress on the undrained cyclic behavior of saturated sand in which the strain level

[1] Ph.D. Student, Department of Civil Engineering, University of Tokyo
[2] Associate Professor, Institute of Industrial Science, University of Tokyo
[3] Senior Lecturer, Department of Civil Engineering, University of Moratuwa, Sri Lanka
[4] Technical Director, Integrated Geotechnology Institute Ltd.
[5] Professor, Institute of Industrial Science, University of Tokyo

could exceed more than 20 %. In previous studies, in the case of simple shear tests, the shear strain level was limited to 10 % due manly to technical limitation of the employed apparatus (Vaid and Finn, 1979); as well, in the case of triaxial tests, due to larger extents of non-uniform deformation of the specimen at higher strain levels, the axial strain level could not exceed 20 % (Vaid and Chern, 1983; Hyodo et al., 1991, among others).

In view of the above, the purpose of this study is set to better understand the behavior of saturated sand under undrained cyclic loading which leads to liquefaction and extremely large cyclic shear strain development. In this paper, the results from investigations on the effect of initial shear stress on the undrained cyclic behavior of saturated Toyoura sand subjected to cyclic torsional shear loading up to single amplitude of shear strain of about 50 % under various combinations of static and subsequent cyclic shear stresses are presented.

TEST APPARATUS AND PROCEDURE

Fig. 1 presents schematically the torsional loading apparatus on hollow cylindrical specimens which was employed in this study. This test device, developed at IIS, is capable of achieving double amplitude torsional shear strain levels exceeding 100 % by using a belt-driven torsional loading system that is connected to an AC servo motor through electro-magnetic clutches and a series of reduction gears; refer to Chiaro et al. (2009) for technical details.

To evaluate large torsional deformations, a potentiometer with a wire and a pulley was employed. The torque and axial load were detected by using a two-component load cell which is installed inside the pressure cell.

The medium-size hollow cylindrical specimens employed were 150 mm in outer diameter, 90 mm in inner diameter and 300 mm in height.
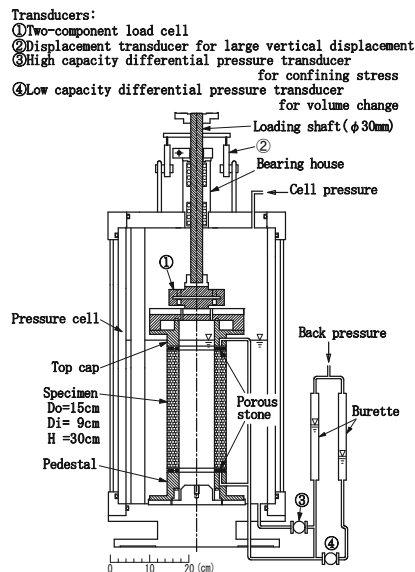
Figure 1   Torsional shear test apparatus on hollow cylindrical specimen

All the tests were performed on Toyoura sand, which is uniform sand with negligible fines content (Table 1). Several specimens with relative density Dr^{40kPa} of about 45 %, as defined at an effective confining stress of 40 kPa, were prepared by air pluviation method. To minimize the degree of inherent anisotropy in radial direction of hollow cylinder sand specimens, sample preparation were carried out carefully by pouring the air-dried sand particles into a mold while moving radially the nozzle of pluviator and at the same time circumferentially in alternative directions, i.e., first in clock-wise and then anti clock-wise directions (De Silva et al., 2006). In addition, to obtain specimens with highly uniform density the falling height was kept constant throughout the pluviation process.

After being saturated, the samples were isotropically consolidated by increasing the effective stress state up to 100 kPa, with a back pressure of 200 kPa. Subsequently, the stress state was changed by applying drained monotonic torsional shear stress up a specified value. Finally, undrained cyclic torsional loading, with constant amplitude of shear stress was applied at a constant shear strain rate of 2.5 %/min.

As listed in Table 2, cyclic loading tests were performed over a wide range of initial static shear varying from 0 to 20 kPa. Two levels of cyclic shear stress, 16 kPa and 20 kPa, were employed in this study in order to consider various combinations of initial static and cyclic shear stresses.

The loading direction was reversed when the amplitude of combined shear stress, which was corrected for the effect of membrane force, reached the target value. During the process of undrained cyclic torsional loading the vertical displacement of the top cap was not allowed with the aim to simulate as much as possible the simple shear condition that ground undergoes during horizontal excitation.

The membrane force was evaluated by conducting a special test which consists in filling water in between outer and inner membranes and shearing cyclically the water specimen under undrained condition up to single amplitude shear strain of 50 %, as explained in detail by Chiaro et al. (2009).

Table 1 Material properties

Material	Specific gravity, Gs	Max. void ratio, e_{max}	Min. void ratio, e_{min}	Mean diameter, D_{50} (mm)	Fines content, F_C (%)
Toyoura Sand	2.656	0.992	0.632	0.16	0.1

Table 2 Test conditions

Test	Relative density, Dr^{40kPa} (%)	Cyclic shear stress, τ_{CL} (kPa)	Static shear stress, τ_{ST} (kPa)	Combined shear stress, $\tau_{max} = \tau_{ST} + \tau_{CL}$ (kPa) $\tau_{min} = \tau_{ST} - \tau_{CL}$ (kPa)	Type of loading
16-00	46.4	16	0	+16 / -16	Reversal
16-05	45.5	16	5	+21 / -11	Reversal
16-10	46.6	16	10	+ 26 / -6	Reversal
16-15	44.2	16	15	+ 31 / -1	Reversal
16-16	46.5	16	16	+32 / 0	Intermediate
16-17	47.9	16	17	+33 / +1	Non-Reversal
16-20	45.3	16	20	+36 / +4	Non-Reversal
20-00	48.1	20	0	+20 / -20	Reversal
20-05	48.0	20	5	+25 / -15	Reversal
20-10	45.6	20	10	+30 / -10	Reversal
20-15	44.4	20	15	+35 /-5	Reversal
20-20	46.9	20	20	+40 / 0	Intermediate

The shear stress τ is corrected for effect of membrane force. The cyclic shear stress is applied under undrained condition, while preventing any vertical displacement of top cap.

Reversal, intermediate and non-reversal loading tests

During each cycle of loading in some tests, the combined shear stress value is reversed from positive $(\tau_{max} = \tau_{ST} + \tau_{CL} > 0)$ to negative $(\tau_{min} = \tau_{ST} - \tau_{CL} < 0)$, or vice versa; this type of loading is called hereafter as reversal loading; whereas, the type of loading in which the reversal of loading direction is made when the value of combined shear stress (τ_{min}) achieves zero during the undrained torsional shear loading is called intermediate loading; and the one in which the combined shear stress is always kept positive is called non-reversal loading.
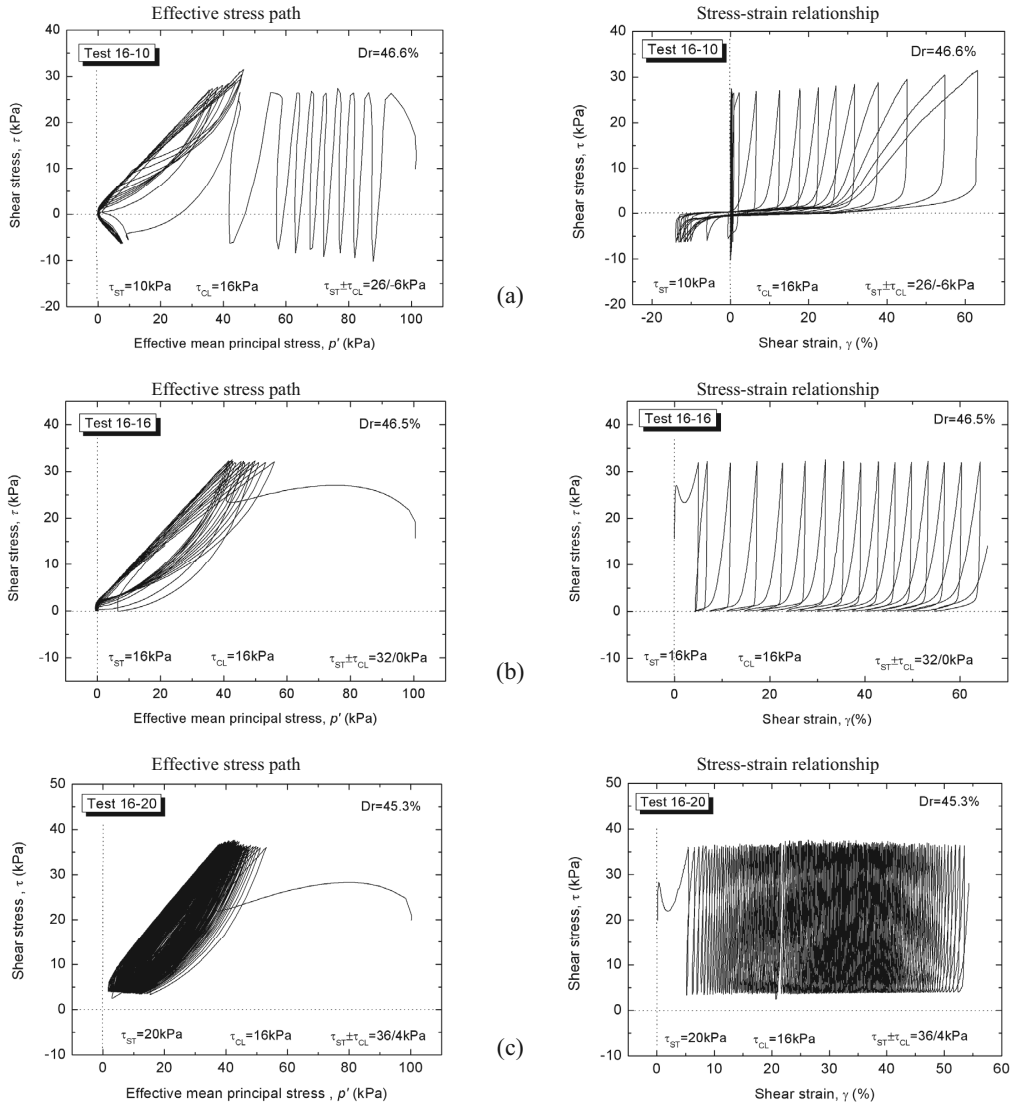
Figure 3   Typical effective stress paths and stress-strain relationships for cyclic torsional shear tests on Toyoura sand: (a) reversal, (b) intermediate, and (c) non-reversal loading

Fig. 3(a) shows typical reversal loading test results (e.g., Test 16-10) in which cyclic mobility was observed in effective stress path, where the effective stress recovered repeatedly after achieving the state of zero effective stress (i.e., full liquefaction). It was accompanied with a significant development of shear strain as evidenced by stress-strain relationship.

Fig. 3(b) illustrates typical intermediate loading test results (e.g., Test 16-16). This type of tests shows behavior that is similar to that of reversal cases, in the sense that after reaching a fully liquefied state, progressive large deformation are developed while showing cyclic mobility. However, it can be distinguished from the reversal one by looking at the failure characteristics, which will be explained later.

Fig. 3(c) represents typical non-reversal loading test results (e.g., Test 16-20). In this case, the state of zero effective stress was not achieved even after applying 208 cycles of loading; even though liquefaction did not occur, a large shear strain level exceeding 50 % was reached, and formation of spiral shear band could be observed.

The results of the above non-reversal loading test indicate that, when the combined shear stress can not achieve the zero state, full liquefaction (i.e., the zero effective stress state) does not occur. However, this does not mean that sand is very resistant against seismic loading; in fact a significant magnitude of combined shear stress may cause failure as evidenced with the formation of shear band.

Effect of static shear on the failure characteristics

In this study, the observed type of failure was distinguished into liquefaction and residual deformation based on the difference in the effective stress path and the modes of development of cyclic residual shear strain during both monotonic and cyclic loading behaviors, as shown schematically in Fig. 4.

In Fig. 4, point A represents the starting point of undrained loading. At point B, cyclic loading begins when the combined stress achieves a specified target value $(\tau_{max}=\tau_{ST}+\tau_{CL})$. Point C represents the full liquefaction state $(p'=0)$. Point D is a reference point for evaluating the level of deformation during cyclic mobility. τ_{peak} is the value of shear stress at peak state during the undrained monotonic loading.

LQ Failure - As indicated in Fig. 4(a), the cyclic loading starts when the shear stress reaches the reversal loading value (τ_{max}), which is lower than τ_{peak}; as a consequence, the stress condition is far from the failure envelope. During the subsequent undrained cyclic loading, while undergoing several tens of cycles, due to the excess pore water pressure generation, the effective mean principal stress progressively decreases and the stress state moves toward to the failure envelope and finally reaches the full liquefaction state $(p'=0)$. Then, in the post liquefaction process, large deformations are easily developed during the cyclic mobility. This type of failure is called hereafter as liquefaction failure (LQ).

RD Failure - As evidenced in Fig. 4(b), the cyclic loading begins when the shear stress reaches the reversal loading value (τ_{max}), which is higher than τ_{peak}; as a consequence, the stress state has already reached the failure envelope. During subsequent cyclic loading, liquefaction is not achieved even after applying many cycles of loading. In fact, if the combined shear is always positive (i.e., non-reversal loading) it can happen that the effective mean principal stress does not reach the zero state (i.e., full liquefaction). This is the case in which residual deformation brings the sample to failure. This type of failure is called hereafter as residual deformation failure (RD).

CL Failure - As shown in Fig. 4(c), the specimen behaves in a manner that is similar to the RD failure with the exception that liquefaction occurs in a few cycle of loading. As a consequence, faster development of residual deformation is obtained. This type of failure, in which liquefaction is combined with residual deformation, is called hereafter as combined liquefaction failure (CL).

In Fig. 5, the results obtained from the above analysis of failure mechanism are illustrated in terms of the combined effects of cyclic stress ratio (τ_{CL}/p_0') and static stress ratio (τ_{ST}/p_0').

In this plot, the Peak Line (PL) is the boundary between LQ and CL failure behaviors and represents the stress condition of $\tau_{max}=\tau_{peak}{}^*$ ($\tau_{peak}{}^*$ is the value of peak stress obtained from undrained

monotonic test, as listed in Table 3); on the other hand, the No Liquefaction Line (NLL) represents the threshold of liquefaction failure and is the boundary between CL and RD failure behaviors. In addition, a forth region can be defined, which could represent the condition of no liquefaction and no failure due to lower levels of combined static and cyclic shear stress.
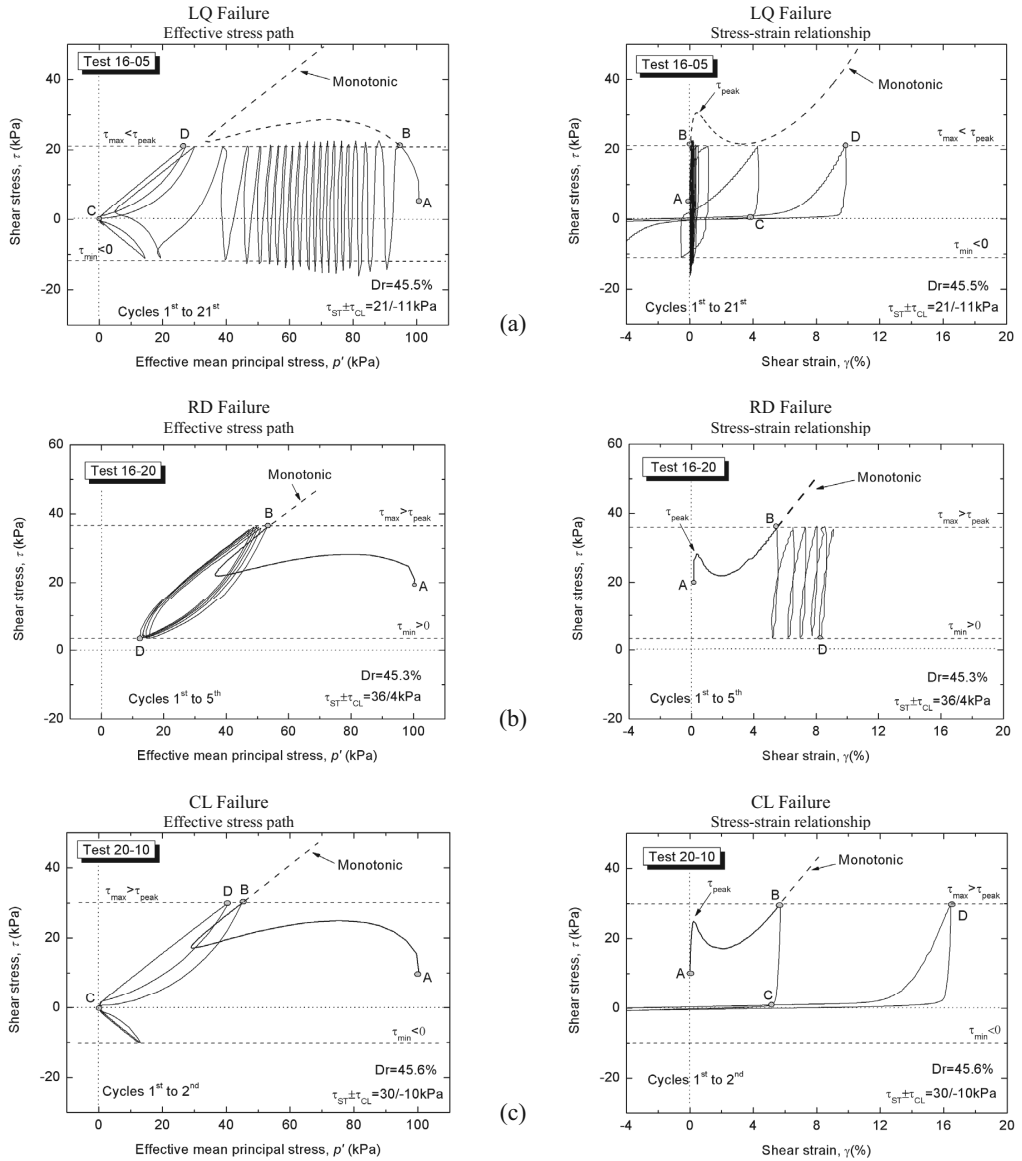
Figure 4 Observed types of failure: (a) liquefaction failure (LQ); (b) residual deformation failure (RD); and (c) combined liquefaction failure (CL).
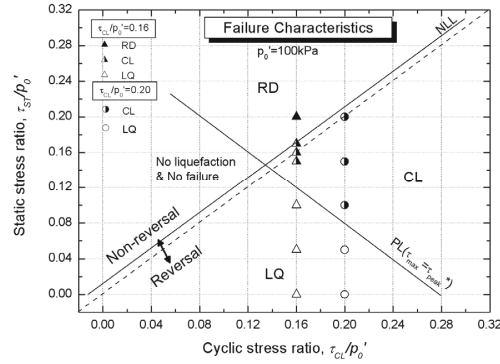
Figure 5 Failure characteristics

Table 3 Liquefaction, strain accumulation and failure characteristics

Test	$\tau_{max}=\tau_{ST}+\tau_{CL}$ (kPa)	τ_{peak} (kPa)	τ_{ST}/p_0'	N_L (p'=0)	N_{10} (γ_{SA}=10%)	N_{50} (γ_{SA}=50%)	Type of failure
16-00	16	28.3*	0	34	36	48	LQ
16-05	21	28.3*	0.05	20	23	33	LQ
16-10	26	28.3*	0.10	10	9	20	LQ
16-15	31	29.2	0.15	2	3	8	CL
16-16	32	27.1	0.16	3	3	13	CL
16-17	33	28.8	0.17	9	4	30	CL
16-20	36	28.3	0.20	No Liq.	8	202	RD
20-00	20	28.3*	0	3	3	18	LQ
20-05	25	28.3*	0.05	2	3	14	LQ
20-10	30	25.0	0.10	0.5	2	8	CL
20-15	35	26.3	0.15	0.5	2	7.5	CL
20-20	40	33.3	0.20	0.5	2	9	CL

* τ_{peak} obtained from undrained monotonic torsional shear test; p_0'=100 kPa

LQ: liquefaction failure; CL: combined liquefaction failure; RD: residual deformation failure

Resistance to liquefaction and cyclic strain accumulation

The effect of initial static shear stress on cyclic behavior of saturated Toyoura sand was evaluated in terms of relationships between the static stress ratio (τ_{ST}/p_0') and the number of cycles to cause fully liquefied stress state of p'=0 (N_L) or specific amounts of single amplitude shear strain (N_{10} and N_{50}), as listed in Table 3.

As indicated in Fig. 6, the presence of static shear does not always lead to an increase in the resistance to full liquefaction; in fact, it can either increase or decrease with increasing the static shear depending on the magnitude of cyclic shear stress, the type of loading and the failure behavior.

At lower levels of static shear (reversal loading tests), the number of cycles required to cause full liquefaction decreases with increasing the static shear level. However a significant reduction in resistance to liquefaction occurs around the PL line with $\tau_{max}=\tau_{peak}$. This change in the liquefaction resistance can be associated with a change in the failure behavior.

After reaching a minimum value of liquefaction resistance in the CL failure region, suddenly the resistance to full liquefaction increases up to the liquefaction threshold (NLL line). This positive increment in the number of cycles to cause full liquefaction can be associated with a change of loading type from reversal to intermediate.

Finally, at higher levels of static shear (non- reversal loading) liquefaction does not occur; in fact, above the NLL line is located the RD failure region which does not allow liquefaction.

It may be noticed that, for a given value of static shear, the resistance to liquefaction decrease with increasing the amplitude of cyclic stress. This response is in accordance with those observed in previous studies, such as Vaid and Finn (1979), Vaid and Chern (1983), Hyodo et al. (1991), among others.
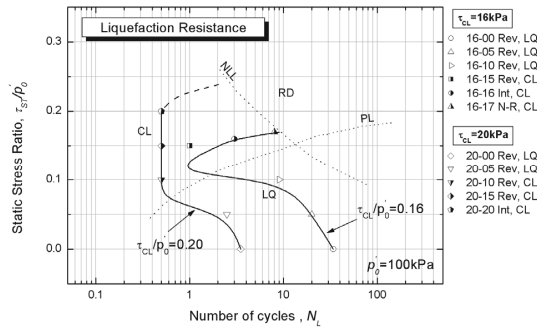
Figure 6 Relationship between static stress ratio and number of cycles to cause full liquefaction (p'=0)
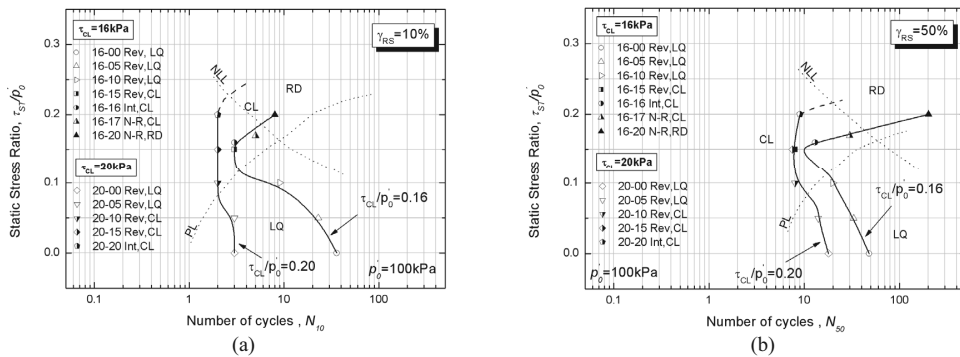
Figure 7 Relationship between static stress ratio and number of cycles to cause: (a) single amplitude shear strain of 10%; (b) single amplitude shear strain of 50%

Figs. 7(a) and 7(b) illustrate the strain accumulation resistance curves for a given value of residual deformation (γ_{RS}) of 10% and 50%, respectively.

Similarly to the liquefaction resistance as described above, the resistance to strain accumulation can either increase or decrease with increasing the static shear depending on the magnitude of cyclic shear stress, the type of loading and the failure behavior.

In fact, at lower levels of static shear (reversal loading tests), the number of cycles required to cause a specified amount of shear strain decreases with the static shear level. Then, a drop in the resistance to strain accumulation occurs around the PL line with $\tau_{max} = \tau_{peak}$. Such change, associated with a change in the failure behavior, is much more significant in the case of lower levels of cyclic stress for shear strain level of γ_{RS}=10%.

Finally, at higher levels of static shear (intermediate and non- reversal loading), after reaching the minimum value of the resistance to strain accumulation in the CL failure region, it increases suddenly

after exceeding the NLL line and entering into the RD failure region.

It may be noticed that, for a given value of static shear, the resistance to strain accumulation decreases with increasing the amplitude of cyclic stress. This response is in accordance with those observed in previous studies, such as Hyodo et al. (1991), among others, in case of moderate levels of deformation.

Residual deformation and strain localization during cyclic loading

In order to examine the effect of initial static shear stress on the cyclic behavior of saturated Toyoura sand, the residual deformation (γ_{RS}) during cyclic loading was measured in terms of single amplitude shear strain (γ_{SA}) at the moment when the combined shear stress recovers the initial value of static shear stress $(\tau = \tau_{ST})$ during the unloading stage of each cycle.

Fig. 8(a) shows the residual deformation behavior of tests characterized by LQ failure. In this type of tests, full liquefaction (i.e., zero effective stress state, $p'=0$) was achieved after applying several cycles of loading and then a sudden development of residual deformation took place.

Fig. 8(b) shows the residual deformation behavior in case of tests in which CL or RD behavior failures were observed. In these types of tests, during the first cycle of loading, the level of residual deformation already reaches a few percent.
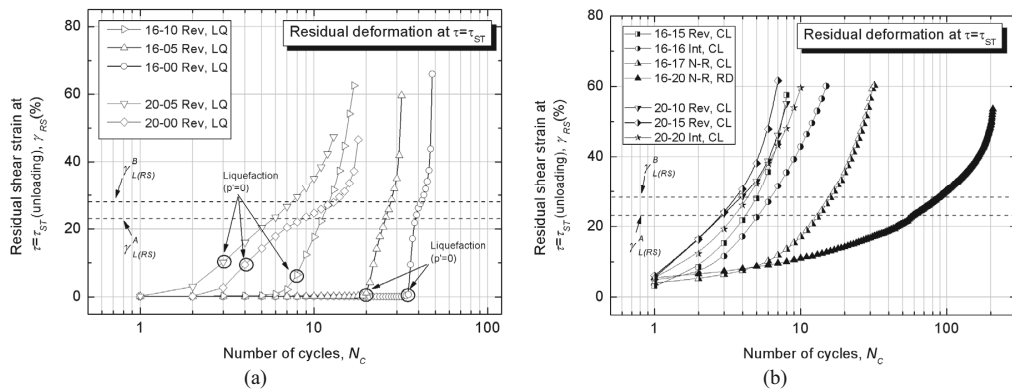
Figure 8 Residual deformation at $\tau = \tau_{ST}$ during the unloading stage of each cycle: (a) LQ failure behavior tests; and (b) CL and RD failure behavior tests

Kiyota et al. (2008) performed undrained cyclic torsional shear tests on saturated Toyoura sand without static shear under different density conditions. Since in their tests the initiation of strain localization could not be clearly defined on the basis of visual observation, they defined it based on the change in the response of the deviator stress $q\ (=\sigma_v' - \sigma_h')$ that was measured during the undrained cyclic torsional shear loading while preventing any vertical displacement of the top cap. The state at which the amplitude of q decreased suddenly was considered at the limiting state to initiate formation of shear band and thus strain localization. In addition, it was accompanied with an increase in the shear increment of single amplitude shear strain $(\Delta\gamma_{SA})$. These features imply that stress-strain characteristics of the specimen were changed by the formation of shear band and the initiation of strain localization in the specimen. As a result, it was found that the limiting state to initiate formation of shear band increases with a decrease in the relative density of the specimen, and it is independent of the level of shear stress ratio (τ_d/σ'_m).

In this study, non-uniform specimen deformations were observed at higher strain levels as shown in Photo 1. Since the effect of initial static shear stress on the limiting state of the uniform specimen deformation (i.e., beginning of strain localization) could not be clearly defined based on visual

observation, the attempt made by Kiyota et al. (2008) was employed. Therefore, from the analysis of deviator stress responses and stress-strain relationships (refer to Fig. 9 and Fig. 10), for all the tests, it was defined: a) the state at which q suddenly decreases (state A); and b) the state at which a change in strain accumulation was observed (state B).
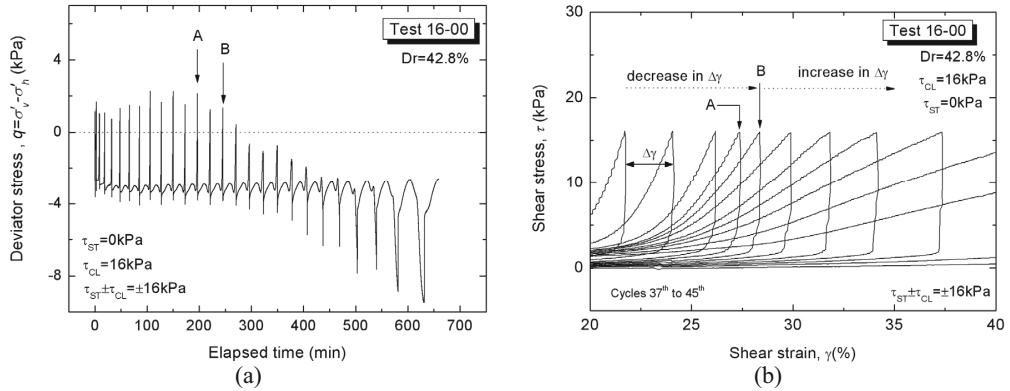
Figure 9 Reversal loading test 16-00: (a) time history of deviator stress, and (b) change in shear strain development during cyclic loading
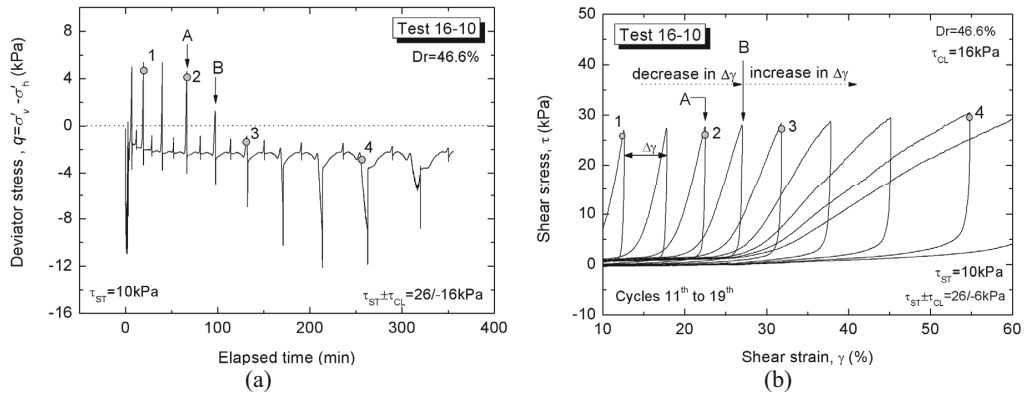
Figure 10 Reversal loading test 16-10: (a) time history of deviator stress, and (b) change in shear strain development during cyclic loading (refer to Photo 1 for specimen deformation at states 1 through 4)

In Fig. 11 and Fig. 12, the value of strain at state A and state B, respectively, was measured in terms of half the double amplitude shear strain ($\gamma_{L(DA)}/2$), as employed by Kiyota et al. (2008), and residual shear strain ($\gamma_{L(RS)}$) (i.e., single amplitude shear strain) which in this study was introduced to better describe the deformation behavior of soil subjected to an initial static shear. In general it was observed that $\gamma_{L(RS}$ shows a less dependence on the levels of static stress ratio (τ_{ST}/p_0') and cyclic stress ratio (τ_{CL}/p_0'). Whereas, $\gamma_{L(DA)}/2$ clearly shows a dependence on both τ_{ST}/p_0' and τ_{CL}/p_0' levels, since it decreases with an increase in τ_{ST}/p_0' and decreases with a decrease in τ_{CL}/p_0'. Therefore, in this study the limiting value to uniform deformation and change in strain accumulation were defined in terms of t $\gamma_{L(RS)}$.

As summarized in Fig.11, in the case of reversal loading tests, based on the change in deviator stress response (state A), the limiting strain value to begin the specimen strain localization could be observed at a $\gamma_{L(RS)}$ level of about 23%; it was identified as $\gamma^A_{L(RS)}$.

On the other hand, as shown in Fig. 12, in case of reversal loading tests, an increase in the single amplitude shear strain $(\Delta\gamma_{SA})$ during each cycle was observed at shear strain level of about 28%. Such change in strain accumulation (state B) was identified as $\gamma^B_{L(RS)}$.

It should be noted that, in case of intermediate and non-reversal loading tests it was not possible to define a clear limiting value to initiate the strain localization and change in strain accumulation.
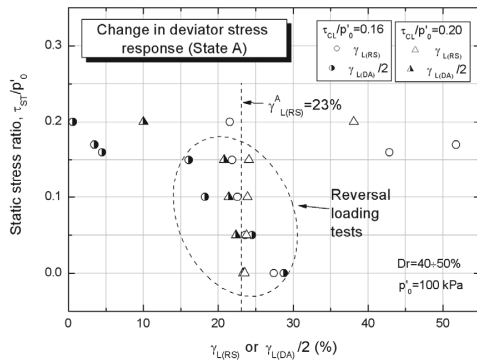
Figure 11 Observed change in deviator stress responses (state A)
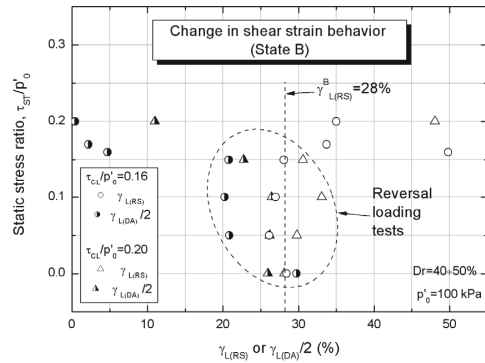
Figure 12 Observed change in strain accumulation responses (state B)

(a) state 1 (γ=12%) (b) state 2 (γ=22%) (c) state 3 (γ=31) (d) state 4 (γ=54%)
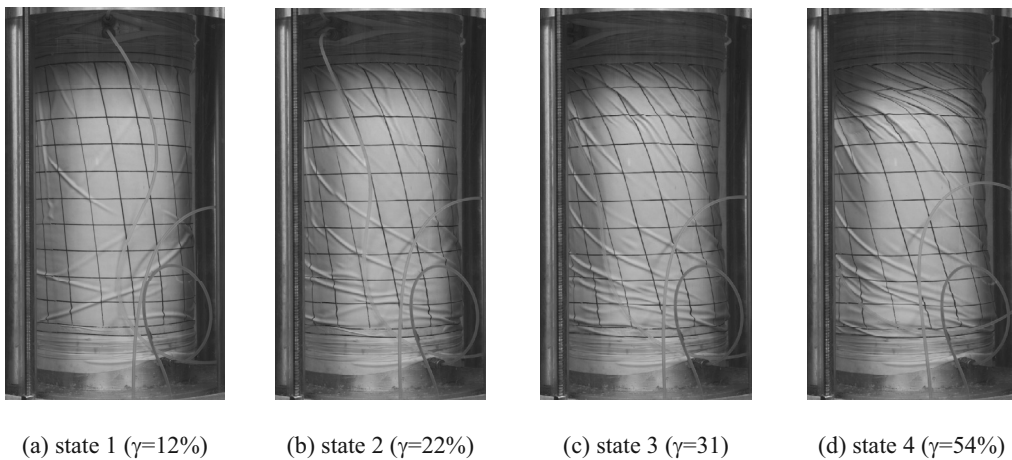
Photo 1 Specimen deformation at states 1 through 4 shown in Fig. 10
(refer to Fig. 10 for deviator stress response and stress-strain behavior at states 1 through 4)

Specimen deformation at several states as numbered 1 through 4 in Fig. 10 is shown in Photo 1. At state 1 (γ = 12%), the deformation was almost uniform except for the regions close to the pedestal and the top cap that are affected by the end restraint; the outer membrane appeared slightly wrinkled. At

state 2 ($\gamma= 22\%$), the outer membrane was visibly wrinkled; in the region near the top cap the deformation of the specimen started to localize due probably to water film formation. At state 3 ($\gamma=31\%$), the localization of specimen deformation developed clearly in the upper part of the specimen. At state 4 ($\gamma=54\%$), the specimen was almost twisted near the top cap.

CONCLUSIONS

With the aim to better understand the role which the static shear plays on the undrained cyclic behavior of saturated sand, a series of undrained cyclic torsional shear tests was conducted on saturated Toyoura sand specimens up to single amplitude of shear strain of about 50 % under various combinations of static and subsequent cyclic shear stresses.

Depending on the magnitude of combined static and cyclic shear stress, the loading pattern could be classified into three groups: stress reversal, intermediate and non-reversal.

From the study of failure mechanisms, the observed types of failure could be distinguished into liquefaction and residual deformation based on the difference in the effective stress path and the modes of development of shear strain. In case of stress reversal and intermediate loadings, failure was associated with full liquefaction, followed by extremely large deformation during cyclic mobility. Whereas, in the case of non-reversal loading, it was found that residual deformation brought the specimen to failure (i.e., formation of spiral shear band) although liquefaction did not occur.

The test results show that the presence of static shear does not always lead to an increase in the resistance to liquefaction and strain accumulation; in fact, both can either increase or decrease by increasing the static shear depending on the magnitude of the combined shear stress, the type of loading and the failure behavior.

In this study, the limiting state of uniform specimen deformation (i.e., strain localization) could not be clearly defined based on visual observation, therefore the state at which amplitude of q decreased suddenly (state A) was considered at the limiting state to initiate formation of shear band and thus strain localization. It was accompanied with an increase in the shear increment of single amplitude shear strain (state B).

REFERENCES

Chiaro, G., Kiyota, T., De Silva, L.I.N., Sato, T., and Koseki, J. (2009): "Effect of static shear on undrained cyclic behavior of saturated sand", *Bulletin of ERS,* Institute of Industrial Science, University of Tokyo, **42**, 63-71

De Silva, L.I.N., Koseki, J., and Sato, T. (2006): "Effects of different pluviation techniques on deformation property of hollow cylinder sand specimens", *Proc. of the International Summer Symposium on Geomechanics and Geotechnics of Particulate Media*, Ube, Yamaguchi, Japan, 29-33

Hamada, M., O'Rourke, T.D. and Yoshida, N. (1994): "Liquefaction-induced large ground displacement", *Performance of Ground and Soil Structures during Earthquakes, 13th ICSMFE*, JGS, 93-108

Hyodo, M., Murata, H., Yasufuku, N., and Fujii, T. (1991): "Undrained cyclic shear strength and residual shear strain of saturated sand by cyclic triaxial tests", *Soils and Foundations*, **31**(3), 60-76

Kiyota, T., Sato, T., Koseki, J., and Mohammad, A. (2008): "Behavior of liquefied sands under extremely large strain levels in cyclic torsional shear tests", *Soils and Foundations*, **48** (5), 727-739

Vaid, Y.P. and Finn, W.D.L. (1979): "Static shear and liquefaction potential", *Journal of the Geotechnical Engineering Division*, Proc. ASCE, **105** (GT10), 1233-1246

Vaid, Y.P. and Chern, J.C. (1983): "Effects of static shear on resistance to liquefaction", *Soils and Foundations*, **23**(1), 47-60